Astron. Astrophys. 321, 105–110 (1997)

ASTRONOMY
AND
ASTROPHYSICS

Radio spectra of Gigahertz Peaked Spectrum radio sources

W.H. de Vries[1,2], **P.D. Barthel**[1], **and C.P. O'Dea**[2]

[1] Kapteyn Astronomical Institute, P.O.Box 800, 9700 AV Groningen, The Netherlands
[2] Space Telescope Science Institute, 3700 San Martin Drive, Baltimore, MD 21218, USA

Received 19 October 1995 / Accepted 18 October 1996

Abstract. A well defined sample of 72 Gigahertz Peaked Spectrum radio sources is compiled, having turnover frequencies in the range of 0.5 – 10 GHz. Using this sample, the canonical GPS radio spectrum is constructed, which is found to have a constant shape, independent of AGN type, redshift or radio luminosity. A possible deficiency of low turnover frequencies at high redshift is found, which may reflect a physical mechanism where turnover frequency and radio luminosity are correlated.

Key words: galaxies: active – radio continuum: galaxies – quasars: general

1. Introduction

Gigahertz Peaked Spectrum (GPS) radio sources, having pronounced radio spectral curvature around 1 GHz, are very powerful radio emitters with total isotropic radio luminosities up to 10^{45} ergs s^{-1}, comparable to the most luminous quasars. This makes them useful probes of the early universe. Their radio morphology is unlike that of classical extended (core dominated or edge brightened) radio sources: GPS sources are invariably compact ($<$1 kpc) and usually only show structure at VLBI resolution scales (e.g. Hodges et al. 1984, Pearson & Readhead 1988, Wilkinson et al. 1994, Dallacasa et al. 1995, Readhead et al. 1996). The resolved structures are double or triple, the components typically separated by a few tens of milliarcseconds. A few GPS quasars presently remain unresolved at milliarcsecond resolution.

Mutel, Phillips and coworkers investigated the nature of the GPS sources with double radio components. They proposed that the "Compact Double" (CD)[1] class of objects are miniature versions of classical extended edge brightened Fanaroff-Riley class 2 (FR II) radio sources (e.g. Phillips & Mutel 1981; Hodges et al. 1984; Mutel & Phillips 1988) and suggested an evolutionary sequence from CD to "Compact Steep Spectrum" (CSS) to FR II objects which has been further modeled by Carvalho (1985), Fanti et al. (1995), Begelman (1995), and Readhead et al. (1996). CSS sources are defined as having subgalactic size (typically $\lesssim$ 20 kpc), and these sources sometimes display turnover frequencies in the 100–300 MHz range (cf. Fanti et al. 1990). Hence CSS sources are different from GPS objects both in spectral shape and radio source dimension. FR II sources constitute the large end of the evolutionary track with sizes up to a few Mpc. Alternatively, the GPS phenomenon could be a permanent phase, in sources with central gas densities high enough to "frustrate" and effectively confine the jets to sub-kpc scales (O'Dea et al. 1991). For some of the GPS sources having extended radio emission ($\approx$ 10% of total sample, cf. Stanghellini et al. 1990, 1997) a recurrent GPS phase, induced by merger or interaction events, was proposed (e.g. Baum et al. 1990, Carvalho 1994). These events will increase the central density, leading to a decrease in jet velocity (a "smothering" of the jets). This temporarily cuts off the energy supply to the previously built up external radio structures, which will subsequently fade in radio luminosity until the jets break free from the confining medium.

GPS sources are identified with galaxies at low to intermediate redshifts ($0.1 \lesssim z \lesssim 1$) and quasars at higher redshifts ($z \gtrsim 1$, cf. O'Dea 1990). Multi-color broad band imaging of the GPS radio galaxies (O'Dea et al. 1996) shows that the host galaxy colors are consistent with non- or passively evolving ellipticals, with absolute magnitudes comparable to brightest cluster members. A similar result has been derived from the R-band Hubble diagram for the GPS galaxies (Snellen et al. 1996). Some of the galaxies, however, show distorted outer isophotes, suggesting an ongoing merger or interaction event (e.g. Stanghellini et al. 1993, O'Dea et al. 1990a). Still a large fraction of the tabulated GPS sources have no optical counterpart ($\approx$ 15%). These empty fields are most likely distant galaxies, presently too faint to detect.

In this paper we investigate the properties of the average radio spectral shape of GPS sources and the evolution of the spectrum with redshift. We derive for a sample of GPS sources typical values for turnover frequency, radio spectral indices, radio luminosities, and angular and physical sizes.

Send offprint requests to: P.D. Barthel

[1] Recently renamed "Compact Symmetric Objects" by Wilkinson et al. 1994 and Readhead et al. 1996.

2. Sample and selection

Our sample of GPS objects was extracted from the working list compiled by O'Dea et al. (1991, with later additions). This list consists of 105 candidate GPS sources, of which 57 have redshift information. Being compiled on the basis of heterogeneous radio spectral data, the list contains objects of mixed GPS quality. From the literature we collected as many radio flux density values at 0.4, 1.4, 2.7 and 5 GHz for the sources as possible, to be used in an assessment of the GPS classification as well as in the construction of a canonical GPS spectrum (Sect. 3.1). Furthermore, we graphically determined the peak radio flux density and observed turnover frequency (ν_T) in those cases where the radio spectrum exhibits a marked peak. This determination was not always possible since some of the radio spectra are undersampled; these sources are not included further in our investigation. On the remaining GPS candidate sources we placed the following constraints: 1) the observed turnover frequency has to be in the window 0.5 to 10 GHz; 2) the measured spectral curvature (the difference between the spectral indices below and above the peak) has to be larger than 0.6. These constraints removed a few CSS sources (notably 1634+628 (3C 343) and 1637+626 (3C 343.1)) with low turnover frequencies ($\nu_T \approx 0.3$ GHz) and a few GPS candidates (e.g. 0615+820, 1351−018 and 1601−222) with very broad peaks and ill defined maxima. The resulting sample of 72 bona fide GPS objects with their spectral indices is listed in Table 2; 38 sources have a redshift measurement. Most of the further discussion will focus on these 38 sources with redshift information; only the canonical spectrum is constructed with the complete subsample of 72 sources (Sect. 3.1).

3. Sample properties

In Fig. 1 we plot the intrinsic turnover frequency as a function of redshift, using the data from Table 2. Because the observed peak frequency in our sample is defined to fall in the $0.5 - 10$ GHz range, the intrinsic frequency range grows with a $(1 + z)$ factor. This window is marked with the dashed lines in the figure. We are therefore locally excluding sources we would include at higher redshifts and vice versa. On top of this sample exclusion effect, one sees a trend towards higher turnover frequencies at higher redshifts. The resulting "gap" between the solid line (an eyeball fit) and the lower dashed line indicates this effect.

Even though there is a small redshift overlap in the GPS quasar and GPS galaxy distributions, we feel confident that we are dealing with a homogeneous sample, at least as far as the radio properties are concerned (cf. Sect. 3.1).

Previous work done by Menon (1983) suggested a strong correlation between turnover frequency and redshift for a small sample composed mostly of CSS quasars. His work indicated an increase in turnover frequency with redshift. For our sample of GPS quasars and GPS galaxies, we find no evidence for this strong correlation, only the possible absence of low ν_T sources at high z. However, since our and Menon's sample selection criteria were different, our results do not necessarily contradict his. Further study of a larger sample of CSS sources is needed.

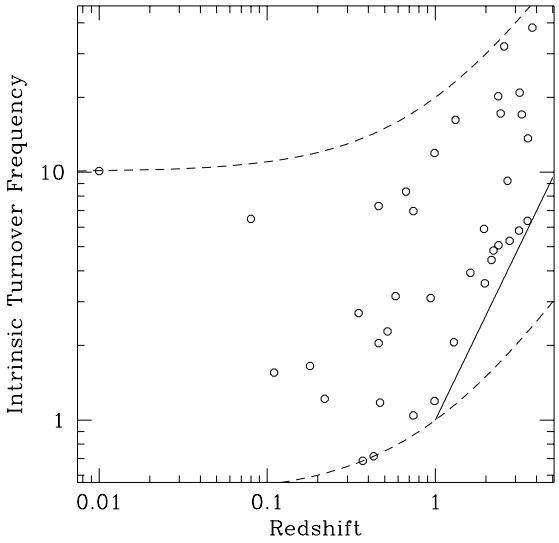

Fig. 1. Intrinsic turnover frequency vs. redshift. The dashed lines indicate sample exclusion lines at $\nu_{T,observed}$ = 0.5 and 10 GHz. The solid line indicates an eyeball fit to the minimum turnover frequency at a certain redshift.

Concerning the apparent absence of low ν_T sources at high z we note that some of the EF objects in our list, if located at $z \gtrsim 2$ would fill in the gap in Fig. 1. This gap can also be filled by weak, presently undetected low ν_T sources at high z. These sources, however, do not belong to the high radio power GPS population for which a correlation between radio luminosity and ν_T may be present as we will argue in Sect. 3.2.

3.1. Canonical radio spectrum

In order to address the consistency of the radio spectral shape of our sample sources, we construct a canonical radio spectrum for these objects. The limited scatter in datapoints (cf. Fig. 2) is indicative of this consistency. Also, by including redshift information in this plot, we are able to check for evolutionary effects on the spectral shape, using two distinct redshift bins. This can furthermore distinguish between spectral shapes of GPS quasars and galaxies, due to their distinct redshift distributions. In the following paragraph the construction method is described.

Normalizing the observed frequencies and fluxes by the source peak frequency and peak flux density allows comparison between the sources dealing with the shape of their radio spectra. In Fig. 2 we plot these relative fluxes and frequencies. Note that theoretically all sources have to go through the point (ν/ν_T=1 , $S(\nu)/S(\nu_T)$=1). The variations in the literature flux measurements (even at the same frequency) and uncertainty in the graphically determined maxima cause a slight scatter around this point. We model the spectral form by three lines, each a least squares fit to the data. The optically thick (low frequency) side can be adequately fitted by one line. A two line fit, such as fit-

Table 1. Spectral fits for different redshift bins

Redshift range	fit	Redshift range	fit
0 – 1	-0.55 ± 0.04	1 – 4	-0.56 ± 0.05
	0.45 ± 0.02		0.52 ± 0.04
0 – 2	-0.52 ± 0.04	2 – 4	-0.63 ± 0.05
	0.48 ± 0.03		0.45 ± 0.04

ted to the high ν side, yields two equal spectral indices. The short middle line indicates the relative flatness of the spectrum in the range of ν_{peak} to $2\nu_{peak}$. This flatness is consistent with the notion that GPS sources consist of a few (two in case of the CD-subclass) components with slightly differing peak frequencies; the addition of the component spectra results in a broader peaked spectrum. The increased scatter at low relative frequencies can either be caused by the presence of optically thin radio emission, external to the GPS self absorbed components, or to the presence of source inhomogeneities and/or multiple self absorbed components. The spectral indices [2] are (-0.51 ± 0.03) for the optically thick side (below peak); (0.36 ± 0.05) for the flat part; and (0.73 ± 0.06) for the optically thin part. The smaller error in the first spectral index is due to the larger number of data points compared to the two other fits. The optically thin spectral index is close to the typical value for large scale FR II sources of 0.75 (e.g. Pauliny-Toth & Kellermann 1972). The mean spectral curvature for GPS sources between a tenth and ten times the peak frequency is found to be 1.24 ± 0.07.

The sample is now further subdivided in redshift bins of $[0, 1]$ and $\langle 1, 4]$ to search for possible differences between GPS galaxy and quasar radio spectra. A redshift binning of $[0, 2]$ and $\langle 2, 4]$ is used to detect redshift evolution of spectral form. The results are listed in Table 1. We used a two component fit to the spectra in order to avoid bins with a low number of data points. This results in a slightly lower value of the spectral index at the optical thin side compared to the value found in Sect. 3.1 The absence of any significant trend has twofold implication: 1) the GPS quasars and radio galaxies in our sample are not different in the shape of their radio spectra, 2) the GPS spectral shape is constant over at least 3 orders of magnitude in radio luminosity (and therefore constant with redshift).

3.2. Turnover frequency vs. radio luminosity

The redshift versus turnover frequency plot (Fig. 1) shows a possible deficiency of low ν_T's at higher redshifts. This gap can be filled in by high z GPS sources with low ν_T's. In order to discriminate between the high power – low ν_T sources which should have been detected and the currently overlooked low power – low ν_T sources, we consider the relationship between radio luminosity and turnover frequency. As most of the sources have peak flux densities in the 1 Jy regime, their intrinsic radio power scales rather well with redshift. This leads to a similar plot as in Fig. 1 with the important difference that the gap in Fig. 3 will not be filled in by the postulated currently undetected population of low luminosity low ν_T GPS objects: this population will be located in the left part of the diagram. From our sample list, none of the sources without redshift information will end up in the gap at any $z \lesssim 5$, either because their intrinsic turnover frequency will become too large at high z, or because their radio spectral indices are too steep to attain high enough radio powers. In Fig. 3, the dashed lines are the frequency exclusion limits, plotted using the tight correlation between radio power and redshift. The upper limit is normalized using the 10 GHz point at 10^{34} W (@ z = 0.01) [3]; the lower limit at the 2.5 GHz point at 10^{40} W (@ z = 4). These lines are similar to the dashed lines in Fig. 1. Sources with intermediate radio luminosities and high intrinsic turnover frequencies (falling above the top dashed line), as well as very high power radio sources with low (< 0.5 GHz) ν_T's (below the bottom dashed line) are excluded from our sample via selection on observed turnover frequency.

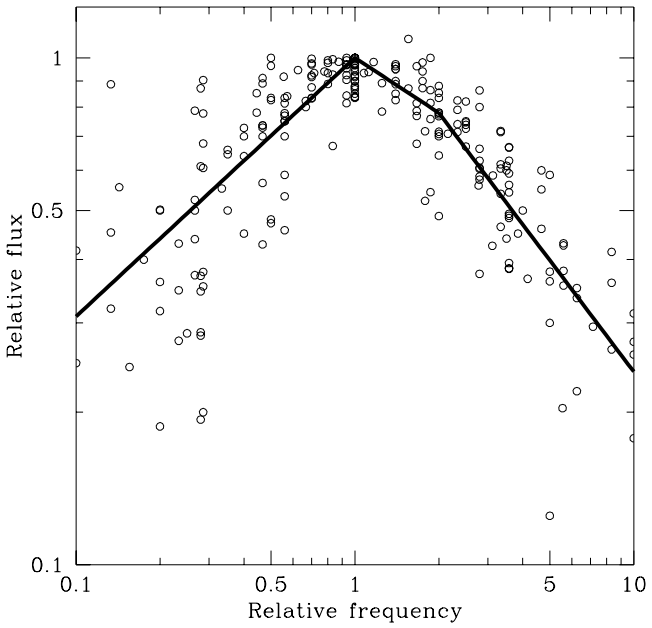

Fig. 2. Canonical GPS spectrum. The least squares fits to the data have the following indices: $\nu \leq \nu_T$: (-0.51 ± 0.03); $\nu_T < \nu \leq 2\nu_T$: (0.36 ± 0.05); $\nu > \nu_T$: (0.73 ± 0.06). The convention used is: $S \propto \nu^{-\alpha}$.

A substantial part of the sources have been selected from the catalogs of Kühr et al. (1980, 1981). Since the catalogs combined have a completeness limit of 1 Jy at 5 GHz, we might just be biased against sources with ν_T's significantly differing from the 5 GHz selection frequency. Due to the spectral shape these sources would be too faint to end up in the initial catalog, even though a lot of sources below 1 Jy are included, it is still not complete to that level. To see how this affects the results plotted in Fig. 3, we calculated completeness limits as a function of radio luminosity. Since sources at high redshifts and with observed ν_T's of 0.5 to 1 GHz would fill in the gap, we plotted curves for observed turnover frequencies of 0.5 (bottom

[2] We use the convention S $\propto \nu^{-\alpha}$ throughout this article

[3] We use H_0 = 75 km s^{-1} Mpc^{-1} and q_0 = 0.5 throughout this paper

Table 2. Spectral indices of bona fide GPS sources

(1) Source	(2) ID	(3) z	(4) S_T	(5) ν_T	(6) α_{thick}	(7) α_{thin}	(8) Sp.Cur	(1) Source	(2) ID	(3) z	(4) S_T	(5) ν_T	(6) α_{thick}	(7) α_{thin}	(8) Sp.Cur
0018+729	G		1.0	0.6	−0.55	0.48	1.03	1323+321	G	0.37	7.5	0.5	−0.40	0.50	0.90
0019−000	G		3.1	0.8	−0.37	0.57	0.94	1333+459	Q	2.45	0.8	5.0	−0.98	0.88	1.86
0022−423	G	0.94	2.9	1.6	−0.90	0.47	1.37	1354−174	Q	3.15	1.5	1.4	−0.40	0.32	0.72
0039+230	EF		0.9	2.8	−0.30	1.12	1.42	1355+441	EF		0.8	2.0	−0.37	0.35	0.72
0108+388	G	0.67	1.3	5.0	−0.39	0.54	0.93	1358+624	G	0.43	6.5	0.5	−1.40	0.56	1.96
0144+209	EF		1.2	1.3	−0.63	0.59	1.22	1404+286	G	0.08	3.0	6.0	−0.85	0.51	1.36
0159+839	S		0.2	5.0	−0.47	0.91	1.38	1442+101	Q	3.54	2.5	1.4	−0.08	0.56	0.64
0201+113	Q	3.56	1.3	3.0	−0.57	0.52	1.09	1518+047	Q	1.29	5.4	0.9	−0.20	0.93	1.13
0237−233	Q	2.22	7.0	1.5	−0.49	0.64	1.13	1519−273	S		2.4	5.0	−0.11	0.66	0.77
0238−084	G	0.01	3.0	10	−0.40	1.33	1.73	1600+335	G		1.5	1.2	−0.06	0.76	0.82
0248+430	Q	1.32	1.5	7.0	−0.43	0.53	0.96	1604+315	G		0.9	1.5	−0.59	0.28	0.87
0316+161	G		10	0.7	−0.31	0.62	0.93	1607+268	G	0.47	5.0	0.8	−1.08	0.60	1.68
0428+205	G	0.22	4.0	1.0	−0.35	0.33	0.68	1732+094	G		1.2	2.8	−0.70	0.57	1.27
0437−454	S		1.5	5.0	−0.34	0.71	1.05	1751+278	G		0.6	1.4	−0.27	0.57	0.84
0457+024	Q	2.38	2.0	1.5	−0.52	0.42	0.94	1824+271	?		0.4	1.0	−0.39	0.75	1.14
0500+019	G	0.58	2.6	2.0	−0.63	0.32	0.95	1843+356	G		1.0	2.0	−1.00	0.22	1.22
0507+179	S		1.3	1.4	−0.77	0.45	1.22	1848+283	Q	2.57	1.1	9.0	−0.52	0.99	1.51
0528−250	Q	2.77	1.5	1.4	−1.28	0.37	1.65	1851+488	S		0.7	3.0	−1.11	0.40	1.51
0552+398	Q	2.37	4.8	6.0	−0.73	0.24	0.97	1934−638	G	0.18	17	1.4	−0.78	0.73	1.51
0554−026	G		0.8	1.0	−1.07	0.63	1.70	2000−330	Q	3.78	1.1	8.0	−0.53	0.65	1.18
0602+780	G		0.2	5.0	−0.58	0.57	1.15	2008−068	G		2.7	1.4	−0.31	0.56	0.87
0636+680	Q	3.18	0.6	5.0	−0.99	0.53	1.52	2050+364	G	0.35	5.1	2.0	−0.43	0.44	0.87
0646+600	Q	0.46	0.9	5.0	−0.39	0.88	1.27	2121−014	G		1.8	0.5	−0.56	0.75	1.31
0710+439	G	0.52	2.2	1.5	−0.75	0.28	1.03	2126−158	Q	3.27	1.2	4.0	−0.60	0.51	1.11
0711+356	Q	1.62	1.8	1.5	−0.62	0.40	1.02	2128+048	G	0.99	5.0	0.6	−0.48	0.42	0.90
0742+103	EF		4.0	3.0	−0.39	0.63	1.02	2149+056	G	0.74	1.2	4.0	−0.38	1.09	1.47
0743−006	Q	0.99	2.0	6.0	−0.42	0.30	0.72	2236+124	S		0.7	5.0	−0.50	0.84	1.34
0802+212	EF		1.0	1.8	−0.54	0.57	1.11	2322−040	G		1.3	1.4	−0.42	0.75	1.17
0858−279	Q	2.16	2.4	1.4	−0.83	0.41	1.24	2323+790	G		1.2	1.4	−0.30	0.75	1.05
0902+490	Q	2.69	0.8	2.5	−0.42	1.04	1.46	2333−528	G		2.3	1.5	−0.18	0.51	0.69
0904+039	EF		1.0	0.8	−0.23	0.83	1.06	2337+264	G		1.2	2.0	−0.71	0.31	1.02
0941−080	G		4.5	0.5	−0.50	0.59	1.09	2342+821	Q	0.74	5.0	0.6	−0.55	0.62	1.17
1031+567	G	0.46	2.0	1.4	−0.47	0.32	0.79								
1100+223	EF		0.7	3.0	−0.25	0.47	0.72								
1118−056	EF		1.1	0.9	−0.31	0.50	0.81	Rejected sources (spectral curvature too low):							
1133+432	EF		1.4	1.0	−0.60	0.60	1.20	0615+820	Q	0.71	1.0	5.0	−0.30	0.20	0.50
1143−245	Q	1.95	1.6	2.0	−1.10	0.33	1.43	1351−018	Q	3.71	1.0	3.0	−0.26	0.25	0.51
1225+368	Q	1.97	2.1	1.2	−0.54	0.70	1.24	1413+349	EF		2.0	1.0	−0.11	0.42	0.53
1245+676	G	0.11	0.3	1.4	−1.50	0.46	1.96	1601−222	EF		1.0	0.6	−0.15	0.39	0.45
1312+699	EF		2.0	1.0	−0.87	1.29	2.16	2352+495	G	0.24	2.7	0.9	−0.05	0.29	0.34

one) and 1 GHz (top one). The redshift range is from 0.04 to 4 (beyond the highest z GPS source). To the left of these solid curves sources would drop below the completeness limit.The gap is to the right of both solid lines, so sample incompleteness is not important at these high radio powers. Sources in the gap would need peak flux densities of tens of Jansky's at those low turnovers to enter the gap.

The straight solid line is an eyeball estimate to the minimum turnover frequency at a certain radio power. The line is parameterized by

$$\log(\nu_{T,min}) \approx -23.4 + 0.61 \log(L_{radio}) \quad (1)$$

The possible non-detection of low ν_T GPS sources at high redshift could imply a physical connection between ν_T and radio luminosity. If the spectral turnover is due to free–free absorption the increase in intrinsic turnover frequency follows naturally from the increase in ambient density with redshift. The electron density can be inferred from (cf. Osterbrock 1989)

$$n_e^2 L \approx 3.05 \times 10^6 \tau \left(\frac{T}{10^4}\right)^{1.35} \left(\frac{\nu}{1\mathrm{GHz}}\right)^{2.1} \quad \mathrm{cm}^{-6}\,\mathrm{pc} \quad (2)$$

(with L in pc, T in K and ν in GHz). The electron density would increase from about 1.6×10^3 cm^{-3} to $\sim 6 \times 10^3$ cm^{-3} as the log radio luminosity increases from 38.5 to 40. The temperature

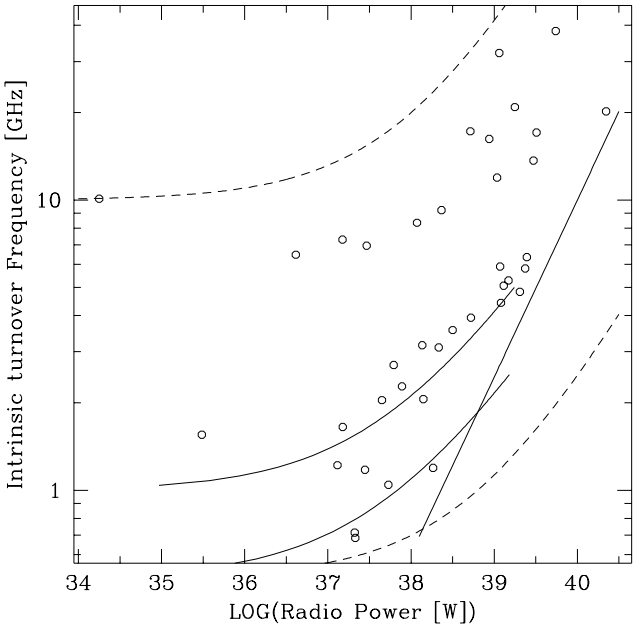

Fig. 3. Intrinsic turnover frequency as a function of radio power. Dashed lines indicate sample exclusion lines due to observed turnover frequency. Solid straight line represents an eyeball fit to the minimum turnover frequency at certain radio power: $\log(\nu_{min})= -23.4 + 0.61 \log(L_{radio})$. Curved solid lines indicate sample completeness thresholds in radio luminosity at observed turnover frequencies of 0.5 and 1 (top curve) GHz, increasing with redshift. To the left (horizontally) of these curves sample incompleteness becomes important. The gap to the right of these curves is therefore unaffected.

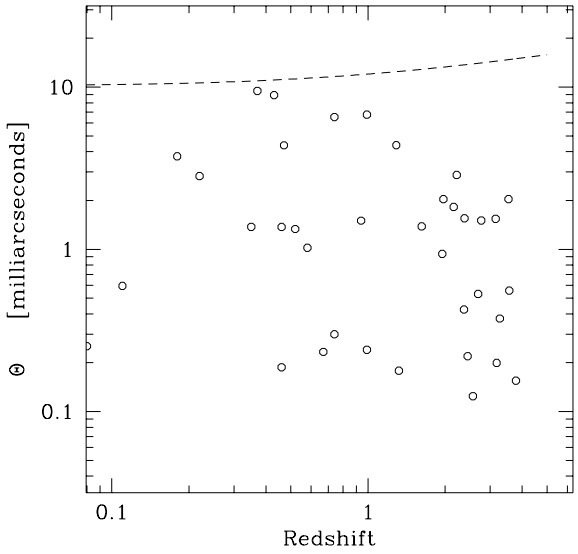

Fig. 4. Angular size of single synchrotron self absorbed systems. vs. redshift. Note that all GPS self absorbed components are smaller than 10 milliarcseconds and at higher redshift become somewhat smaller still. The dashed line indicates redshift evolution of a source with fixed (observed) ν_T = 0.5 GHz and S_T = 10 Jy.

is fixed at 10,000 K, the optical depth is 1 and L is taken to be 10 pc, a typical GPS source component size. The intrinsic turnover frequency is given by Eq. 1. Such densities might be attainable by these high luminosity radio sources, and the total mass contained would be on the order of 1×10^3 $M_\odot$ pc^{-3}. Another possible mechanism is synchrotron self absorption. The self absorbed component sizes inferred from this mechanism are consistent with VLBI measurements of GPS sources, making this the most likely candidate (cf. next section).

3.3. Angular sizes

From the theory on synchrotron self absorption (the mechanism possibly responsible for the radio turnover in GPS sources; cf. O'Dea et al. 1991) an estimate can be made of the angular size of single self absorbed components. Using the correlation between observed ν_T and angular size, as given by Kellermann et al. (1981)

$$\nu_T \approx 8 B^{1/5} S_T^{2/5} \theta^{-4/5} (1+z)^{1/5} \quad (3)$$

(B in Gauss, S_T in Jy, θ in milliarcseconds and ν_T in GHz) and assuming an equipartition magnetic field strength of 100 μGauss (cf. Mutel et al. 1985), we arrive at the following relation:

$$\theta \approx 1.345 \frac{\sqrt{S_T}(1+z)^{1/4}}{\nu_T^{5/4}} \quad (4)$$

Note that if the GPS source consists of multiple components the individual component flux density will be a fraction of the total flux density. Therefore the component size is usually overestimated and can be regarded as a firm upper limit. Note also that Eq. 4 has no bearing on the overall GPS source size (i.e. the separation between the components). Data for the subsample of 38 bona fide GPS sources with redshifts (cf. Table 2) are plotted in Fig. 4.

No single component of a GPS source has an inferred angular size larger than 10 milliarcseconds. This upper limit is consistent with angular size estimates from VLBI measurements of GPS sources (e.g. Phillips & Mutel 1981, Pearson & Readhead 1988, Dallacasa et al. 1995, Stanghellini et al. 1996). The dashed line in the plot indicates the redshift evolution of a source with fixed (observed) ν_T and S_T. The possible redshift evolution of ν_T (cf. Fig. 1 and Sect. 3.2) translates in this plot into a decrease of the maximal angular size with redshift.

3.4. Physical sizes

Since we know the redshift and implied angular size (Eq. 4) for the sources, we can derive an implied physical size for the self absorbed components. The radio luminosity is readily calculated using source (radio) spectral information and redshift. A possible correlation between radio luminosity and self absorbed component size can therefore be investigated using these data.

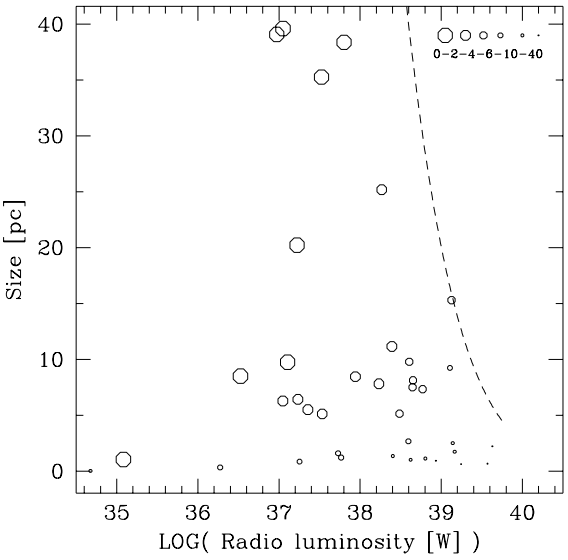

Fig. 5. Inferred source size dependence on radio luminosity (for single components). Circle size indicates intrinsic turnover frequency in GHz. The dashed line indicates evolution of a source along the $\nu_{T,min}$ track (Eq. 1) with S_T fixed at 10 Jy.

The plot is presented in Fig. 5. The circle size indicates the intrinsic turnover frequency. Notice the sharp decline in source size and increase in intrinsic turnover frequency towards higher radio luminosities. The dashed line represents the evolution of a source along the empirical $\nu_{T,min}$ track (Eq. 1) with a constant flux density of 10 Jy. This line forms an upper envelope to the maximal component size at certain radio luminosity. Since the flux density is taken constant, the factor dominating the steep decline in component size is most likely the (observed) turnover frequency. It can be seen that high radio luminosities imply small component sizes. The converse is, however, not the case.

4. Summary and conclusions

We have constructed an improved sample of GPS sources using updated radio spectral information from the literature, thereby reducing the possible contamination by non-GPS sources. Using this subsample we constructed a mean spectrum. The spectral indices derived from the mean radio spectrum are found to have values of $\alpha = -0.51$ below and $\alpha = 0.73$ above peak. Furthermore, we find no difference in spectral index between galaxies and quasars or between low and high redshift sources. A possible deficiency of low ν_T GPS sources at high redshifts (high radio luminosities) is found. This translates into a possible absence of large synchrotron self absorbed components at high radio luminosities, implying a physical correlation between intrinsic turnover frequency and radio luminosity. If, on the other hand, free–free absorption plays an important role in turning over the radio spectrum, a more or less natural explanation for the observed increase in turnover frequency is given by the increase in nuclear density with increasing redshift.

Acknowledgements. This research has made use of the NASA/IPAC extragalactic database (NED) which is operated by the Jet Propulsion Laboratory, Caltech, under contract with the National Aeronautics and Space Administration. We are grateful to Carlo Stanghellini for sharing unpublished data, Ronald Hes for his early contributions to this work, and the referee for useful comments.

References

Baum S.A., O'Dea C.P., Murphy D.W., de Bruyn A.G. 1990, A&A, 232, 19
Begelman M.C. 1995, in "Cygnus A – Study of a Radio Galaxy", eds. C. Carilli and D. Harris, Cambridge University Press, p.209
Carvalho J.C. 1985, MNRAS, 215, 463
Carvalho J.C. 1994, A&A, 292, 392
Dallacasa D., Fanti C., Fanti R., Schilizzi R.T., Spencer R.E. 1995, A&A, 295, 27
Fanti R., Fanti C., Schilizzi R.T., Spencer R.E., Nan Rendong, Parma P., van Breugel W.J.M., Venturi T. 1990, A&A, 231, 333
Fanti C., Fanti R., Dallacasa D., Schilizzi R.T., Spencer R.E., Stanghellini C. 1995, A&A, 302, 317
Hodges M.W., Mutel R.L., Phillips R.B. 1984, AJ, 89, 1327
Kellermann K.I., Pauliny-Toth I.I.K. 1981, ARA&A, 19, 373
Kühr H., Witzel A., Pauliny-Toth I.I.K., Nauber U. 1980, A&AS, 45, 367
Kühr H., Nauber U., Pauliny-Toth I.I.K., Witzel A. 1981, preprint 55, Max Planck Institut f. Radio Astronomie
Menon T.K. 1983, AJ, 88, 598
Mutel R.L., Hodges M.W., Phillips R.B. 1985, ApJ, 290, 86
Mutel R.L., Phillips R.B. 1988, in: The Impact of VLBI on Astrophysics and Geophysics, M.J. Reid and J.M. Moran (eds.), IAU symp. 129, p. 73
O'Dea, C.P. 1990, MNRAS, 245, 20p
O'Dea C.P., Baum S.A., Morris G.B. 1990a, A&AS, 82, 261
O'Dea C.P., Baum S.A., Stanghellini C. 1991, ApJ, 380, 66
O'Dea C.P., Stanghellini C., Baum S.A., Charlot S. 1996, ApJ, 470, 806
Osterbrock D.E. 1989, "Astrophysics of Gaseous Nebulae and Active Galactic Nuclei", University Science Books
Pauliny-Toth I.I.K., Kellermann K.I. 1972, AJ, 77, 797
Pearson T.J., Readhead A.C.S. 1988, ApJ, 328, 114
Phillips R.B., Mutel R.L. 1981, ApJ, 244, 19
Readhead A.C.S., Taylor G.B., Xu W., Pearson T.J., Wilkinson P.N., Polatidis A.G. 1996, ApJ, 460, 612
Snellen I.A.G., Bremer M.N., Schilizzi R.T., Miley G.K., van Ojik R. 1996, MNRAS, 279, 1294
Stanghellini C., Baum S.A., O'Dea C.P., Morris G.B. 1990, A&A, 233, 379
Stanghellini C., O'Dea C.P., Baum S.A., Laurikainen E. 1993, ApJS, 88, 1
Stanghellini C., O'Dea C.P., Baum S.A., Dallacasa D., Fanti R., Fanti C. 1997, in preparation
Wilkinson P.N., Polatidis A.G., Readhead A.C.S., Xu W., Pearson T.J. 1994, ApJ, 432, L87

This article was processed by the author using Springer-Verlag LaTeX A&A style file *L-AA* version 3.